Scilight

Photochemistry and Spectroscopy
https://www.sciltp.com/journals/ps

Article

From Gas-Phase Spectra to Transferable Vitamin Building Blocks: Rotational and Infrared Benchmarks

Vincenzo Barone

INSTM, Via G. Giusti 9, 50121 Firenze, Italy; vincebarone52@gmail.com

How To Cite: Barone, V. From Gas-Phase Spectra to Transferable Vitamin Building Blocks: Rotational and Infrared Benchmarks. *Photochemistry and Spectroscopy* **2026**, *2*(3), 3. https://doi.org/10.53941/ps.2026.100024

Received: 1 June 2026
Revised: 18 June 2026
Accepted: 23 June 2026
Published: 16 July 2026

Abstract: Vitamin-relevant molecular motifs combine heteroatom networks, hydrogen bonds, conjugated polyenes, saturated and fused rings, benzopyran units, and quinone cores. We present an integrated gas-phase validation strategy in which high-resolution rotational spectroscopy and infrared spectroscopy test complementary observables of the same computed structures. Ground-state rotational constants, after anharmonic vibrational correction, provide a quantitative structural anchor through the global mass distribution; gas-phase infrared spectra and tabulated vapor-phase band envelopes probe the local force fields responsible for diagnostic functional-group and fingerprint signatures. Compact fragments are benchmarked against explicitly correlated references, while larger motifs are treated with bond-corrected double-hybrid geometries and validated directly against experiment. The scope is deliberately reference-oriented. Rather than attempting to reproduce physiological condensed-phase environments, the work establishes isolated-molecule benchmarks for tractable vitamins and transferable building blocks for larger, more flexible, or environment-dependent vitamin systems. The protocol is applied to complete vitamin molecules, nicotinic acid and ascorbic acid, and to vitamin-relevant fragments for the vitamin A, vitamin D, vitamin E, and vitamin K families: cyclohexanone, cis-1,3,5-hexatriene, 2-decalone, isochroman, benzoquinone, and naphthoquinone. The rotational benchmark confirms sub-percent accuracy for transferable non-hydrogen-bonded motifs, while the infrared comparisons validate carboxyl, ketone, polyene, and quinone fingerprints. For vitamin C, validation is structural and rotational because no isolated gas-phase infrared spectrum is available. Together, the rotational and infrared tests define a spectroscopic transferability map that separates intrinsic molecular structure from environmental perturbations and provides calibration targets for lower-cost quantum-chemical protocols and molecular-dynamics force fields.

Keywords: rotational spectroscopy; infrared spectroscopy; anharmonicity; molecular structure; vitamins; Pisa Composite Schemes

1. Introduction

Vitamins and their derivatives are compact but chemically demanding molecular systems. Their biological, photochemical, and redox functions depend not only on connectivity, but also on local geometrical details: bond-length alternation in conjugated chains, ring puckering, carbonyl orientation, hydrogen-bond patterns, and heteroatom substitution can all modulate recognition, charge transfer, absorption profiles, and reactivity [1–4]. The same structural coordinates are readily perturbed by solvation, crystal packing, host–guest complexation, or binding to a biomolecular partner. A predictive model must therefore distinguish intrinsic molecular preferences from environment-induced distortions before those effects are recombined in condensed-phase or biological simulations.

Gas-phase high-resolution spectroscopy provides the cleanest route to this intrinsic reference. For an isolated molecule, measured observables can be compared directly with quantum-chemical predictions without solvent, matrix, or packing terms in the model Hamiltonian. Comprehensive reviews of microwave spectroscopy of biomolecular building blocks, broadband rotational spectroscopy, and gas-phase or cryogenic IR/vibrational spectroscopy of biological

molecules and conformers provide the broader experimental context for this strategy [5–11]. The same logic has long been central to high-resolution molecular spectroscopy and to fields such as astrochemistry and atmospheric chemistry, where isolated-molecule fingerprints are indispensable. Its systematic use for medicinal chemistry and biomolecular modeling is more recent, but increasingly important: reference geometries and force fields of this quality are needed to calibrate the lower-cost methods, molecular-mechanics models, and molecular-dynamics force fields used for larger bioactive systems.

No single gas-phase observable is sufficient for this purpose. Pure rotational spectroscopy offers sub-MHz precision and tests the global mass distribution with exceptional sensitivity, but it requires a permanent dipole moment, adequate volatility, and manageable conformational complexity. Infrared and rovibrational spectroscopy can access a broader range of molecular sizes and directly probe local force fields, although band congestion and conformer overlap often make assignments nontrivial. Raman spectra can complement IR data for modes with weak dipole-moment derivatives. In all cases, quantum-chemical calculations are not a post-processing convenience, but an essential part of the spectroscopic analysis: they connect observed lines or envelopes to structures, force constants, anharmonic shifts, and transferable molecular fragments.

The present work adopts this gas-phase reference perspective for vitamin-relevant chemistry. Rotational constants are used as metrological structural anchors because, after vibrational correction, they test the computed equilibrium geometry through the complete mass distribution [12–14]. Infrared spectra examine the same model from a complementary angle: the molecular response to light through local force constants, anharmonic shifts, functional-group positions, and intensity patterns [15–17]. A computed motif that reproduces rotational constants but misses a diagnostic carbonyl, polyene, quinone, or O–H band is structurally plausible, but not yet spectroscopically validated.

This motivates an integrated validation strategy rather than a purely structural benchmark. High-resolution rotational spectroscopy supplies the quantitative anchor, while gas-phase infrared spectra or tabulated band data provide the corresponding light–matter fingerprint [18–20]. The two layers have different strengths: rotational constants yield compact error statistics, whereas IR comparisons reveal whether the validated geometry also generates chemically recognizable local signatures. Together, they define a practical accuracy map for fragment transfer.

Such a map is needed because complete vitamins are not always convenient gas-phase targets. Parent molecules can be too large, too flexible, insufficiently volatile, or too conformationally congested for a complete semi-experimental analysis [18,21,22]. When isolated complete vitamin molecules are experimentally characterized, as in nicotinic acid and ascorbic acid, they provide direct tests of the protocol. For larger vitamin families, the practical route is to validate diagnostic fragments that preserve the local chemistry of the parent scaffold and can later be recombined with quantified uncertainty. The present set therefore combines both situations: nicotinic acid and ascorbic acid are treated as complete vitamin molecules, whereas cyclohexanone, cis-1,3,5-hexatriene, 2-decalone, isochroman, benzoquinone, and naphthoquinone are controlled probes of vitamin A, D, E, and K architectures.

The required theoretical model must be accurate enough for high-resolution spectroscopy and adaptive enough for chemically diverse motifs. Explicitly correlated coupled-cluster approaches can reach the target structural accuracy for compact systems, but their cost grows rapidly [23–25]. Standard density-functional models are affordable, but residual errors in correlation, basis-set incompleteness, core–valence effects, and delocalization can be too large for benchmark use [26–28]. The Pisa Composite Schemes (PCS) address this problem through a hierarchy in which the computational level is matched to molecular size and to the observable being validated [22,23].

This requirement also extends to the nuclear-motion model. The standard rigid-rotor harmonic-oscillator (RRHO) approximation is not sufficient when experimental ground-state rotational constants and diagnostic IR band positions are used as quantitative benchmarks. Second-order vibrational perturbation theory (VPT2) provides a direct link between quantum-chemical force fields and the effective spectroscopic Hamiltonians used to fit experimental rotational and rovibrational data [13,15–17]. In its generalized form (GVPT2), resonant interactions are identified and treated explicitly, yielding accurate anharmonic corrections at a cost compatible with the present molecular sizes, provided that the system is not dominated by pathological large-amplitude modes. Thus, the present protocol is beyond the routine RRHO treatment not only in the electronic-structure model, but also in the vibrational and rotational corrections needed for direct comparison with experiment.

Within this hierarchy, the explicitly correlated PCS2 model supplies reference geometries for compact fragments, whereas the bond-corrected double-hybrid PCS3 (BDPCS3) model extends the same philosophy to larger motifs [26,27]. Equilibrium rotational constants from these structures are converted to ground-state constants with hybrid PCS2 (HPCS2) anharmonic vibrational corrections, so comparison with experiment tests the complete structural prediction rather than the equilibrium geometry alone [14,16,17]. The vibrational layer follows the same logic: HPCS2 anharmonic force fields provide GVPT2 transition lists and rotational vibrational

corrections [13,15,17], while DPCS3 harmonic information is used to diagnose and, where appropriate, improve local force constants in diagnostic regions.

Here we apply this multispectroscopic PCS framework to a curated set of vitamin-relevant molecular motifs: nicotinic acid for vitamin B_3, ascorbic acid for vitamin C, cyclohexanone and cis-1,3,5-hexatriene for vitamin A motifs, 2-decalone for the fused-ring component relevant to vitamin D, isochroman for vitamin E, and benzoquinone/naphthoquinone for vitamin K. The set includes rigid, moderately flexible, and conformationally delicate cases. It tests whether the error reductions observed in broad PCS/Nano-LEGO benchmarks remain valid for vitamin-derived motifs [28,29], and establishes which fragments can be transferred directly, which require local refinement, and which should carry larger uncertainty margins.

The resulting validation layer is designed for use within *Nano-LEGO*, which identifies, extracts, and recombines molecular fragments common in pharmaceuticals and natural products [29]. The goal is to concentrate spectroscopic-level accuracy where it is chemically necessary, then assemble larger vitamin architectures from building blocks whose structural and vibrational reliability has been independently quantified. This reference-to-transfer logic defines the general philosophy of the work: demanding gas-phase calculations establish a validated layer from which simpler quantum-chemical models and molecular-dynamics force fields can inherit reliable local geometries, force constants, and spectral fingerprints.

2. Materials and Methods

2.1. Pisa Composite Schemes

Spectroscopic-level predictions of structures and vibrations require a careful balance between computational cost and theoretical rigor. In complex molecules such as vitamins and their derivatives, different stages of the workflow do not require the same level of precision: equilibrium geometries benefit from the most accurate correlation treatments, whereas later steps, such as vibrational corrections, can be computed with more economical models without appreciable loss of reliability.

The Pisa Composite Schemes (PCS) implement this tiered philosophy by assigning each contribution—valence correlation, core–valence (CV) effects, and basis-set incompleteness—to the most cost-effective theoretical level capable of meeting the target accuracy. All PCS variants use slightly modified cc-pVnZ-F12 (nF12) basis sets [30] for valence contributions and, when needed, cc-pwCVnZ (wCn) basis sets [31] for CV correlation. The variants differ in the electronic-structure method, basis-set size, and treatment of CV contributions.

The geometries of molecules containing up to 20–25 atoms are optimized with the **PCS2** variant. Valence correlation is treated at the CCSD(T)-F12b/2F12$^+$ level, while CV effects are included through second-order Møller–Plesset perturbation theory (MP2)/wC3 all-electron/frozen-core differences:

$$\Delta E^{\mathrm{CV}} = E^{\text{ae-MP2/wC3}} - E^{\text{fc-MP2/wC3}}. \tag{1}$$

The 2F12$^+$ basis set [22,23] is obtained from cc-pVDZ-F12 by adding an f-polarization function to each third-row atom. Numerical gradients with complementary auxiliary basis set (CABS) corrections [32,33] are used for geometry optimization.

For systems larger than about 20–25 atoms, routine PCS2 optimizations become impractical and are replaced by the **BDPCS3** protocol, which offers the most favorable accuracy–cost ratio for large-scale geometry optimizations. It employs a rev-DSD-PBEP86-D3BJ double-hybrid description [34] with a reduced cc-pVTZ-F12 basis set (3F12$^-$) [22], in which the two f-functions of cc-pVTZ-F12 are replaced by a single f-function, as in cc-pVTZ [35]. This underlying electronic-structure level is referred to as DPCS3. Core–valence contributions are not computed explicitly; instead, bond-length adjustments are estimated through an empirical expression involving covalent radii, atomic numbers, and bond-type-specific refinements [27]:

$$\Delta r_{ij}^{BCV} = -k\,[1 + 1.1\,\delta(i,C)\,\delta(j,H)]\,\sqrt{N_i N_j - 1}\,\left(r_i^{cov} + r_j^{cov}\right), \tag{2}$$

where $N = \min(n_i, 3)$, r^{cov} are from Ref. [36], and $k = 0.0011$. A secondary correction, Δr_{ij}^{BV}, is applied to mitigate the residual over-delocalization of semi-local density functionals, and is restricted to specific bonds via Kronecker δ functions and Pauling bond orders:

$$P_{ij} = \exp\left[\frac{r_i^{cov} + r_j^{cov} - r_{ij}}{0.3}\right], \quad P_{ij} > 0.3. \tag{3}$$

Above 50–60 atoms, even the DPCS3 model becomes too costly and is replaced by its cheaper HPCS2

counterpart, which employs the B3LYP-D3BJ hybrid functional with the 6-31+G* basis set. In this case, bond corrections leading to the bond-corrected HPCS2 (BHPCS2) model are obtained with a machine-learning tool based on random-forest regression. HPCS2 is also used to compute vibrational corrections to rotational constants [16,17]; analytical gradients provide the semi-diagonal cubic force constants needed by the GVPT2 framework [13,15]. This choice keeps the residual uncertainty in ΔB_τ^{vib} small relative to the target accuracy of the structural benchmark.

In the tables below, a single method label, such as HPCS2, DPCS3, BDPCS3, or PCS2, denotes equilibrium rotational constants from the corresponding optimized structure. A double-slash label, method1//method2, denotes ground-state rotational constants obtained by adding vibrational corrections computed at method2 to equilibrium constants from method1,

$$B_0(\text{method1//method2}) = B_e(\text{method1}) + \Delta B^{vib}(\text{method2}). \quad (4)$$

Thus, for example, BDPCS3//HPCS2 denotes BDPCS3 equilibrium constants corrected with HPCS2 vibrational contributions. The roles and intended uses of the PCS variants are summarized in Table 1.

Table 1. PCS variants and applications.

Label	Description and Usage
HPCS2	B3LYP-D3BJ/6-31+G*; for anharmonic force field calculations and vibrational corrections.
BHPCS2	HPCS2 + machine-learning bond corrections; equilibrium geometries of very large molecules.
DPCS3	rev-DSD-PBEP86-D3BJ/3F12$^-$; parent level for BDPCS3 structures.
BDPCS3	rev-DSD-PBEP86-D3BJ/3F12$^-$ plus linear corrections for bond lengths; equilibrium geometries of large molecules.
PCS2	CCSD(T)-F12b/2F12$^+$ with CV from MP2/wC3; reference for benchmark geometries and fragment validation.
PCS3	CCSD-F12(T)/3F12 with complete-basis-set extrapolation and refined CV; for high-accuracy single-point energies.

All density functional theory (DFT) and second-order Møller–Plesset perturbation theory (MP2) calculations were performed with GAUSSIAN [37], whereas explicitly correlated computations were carried out through a new interface [24,25] in which the GAUSSIAN geometry optimizer communicates with MOLPRO [38] to evaluate F12 energies. The latest version of this interface is freely available under the MIT license at https://github.com/Ggcri/ExternalGaussianMolproBeta. Bond corrections transforming DPCS3 results into BDPCS3 geometries were applied through the dedicated web interface available at https://www.skies-village.it/proxima/pcsbonds/, which provides a reproducible implementation of the correction protocol.

2.2. Infrared Spectra and Dual-Level Vibrational Comparisons

Anharmonic vibrational calculations used the GVPT2 implementation in GAUSSIAN, in which third and fourth energy derivatives are obtained by finite differences of analytic Hessians. The RRHO model is used only as a zeroth-order reference: the spectroscopic quantities compared with experiment require anharmonic zero-point corrections, resonance-deperturbed vibrational energies, and transition intensities. GVPT2 supplies these terms by combining VPT2 force-field derivatives with an explicit treatment of near-degenerate resonances, which is essential for maintaining a direct connection with the effective Hamiltonians used in experimental analyses. All computed IR transition positions and intensities were taken from GVPT2 line lists, which include both mechanical and electrical anharmonicity. Experimental gas-phase IR traces were taken from National Institute of Standards and Technology (NIST) Chemistry WebBook files in Joint Committee on Atomic and Molecular Physical Data-Digital Exchange (JCAMP-DX) format and normalized to unit maximum absorbance [40]. When only literature band tables were available, as for cis-1,3,5-hexatriene, the reported positions, intensities, and half-widths were converted into a broadened stick spectrum.

For graphical comparison, experimental spectra and computed line spectra were plotted on a common wavenumber axis using Gaussian broadening. Harmonic line spectra were broadened with a full width at half maximum (FWHM) of 18 cm^{-1}, while anharmonic transition lists were broadened with a FWHM of 14 cm^{-1}. The broadened calculated spectra were normalized independently within each panel and mirrored below the experimental trace. This representation emphasizes relative band positions and spectral envelopes rather than absolute intensities, which depend on experimental sampling and on the treatment of electrical anharmonicity.

Unsigned band-position errors were also evaluated for the diagnostic maxima used in the IR discussion. Experimental and calculated band centres were taken from maxima of the normalized broadened profiles within the functional-group and fingerprint windows shown in the figures; for cis-1,3,5-hexatriene, the experimental maxima were obtained from the broadened literature band envelope.

When both HPCS2 anharmonic and DPCS3 harmonic data were available, the comparison was interpreted in a dual-level framework. HPCS2 supplies the GVPT2 transition list, whereas the DPCS3–HPCS2 harmonic differences diagnose the local force-field correction:

$$\nu_i^{\mathrm{dual}} \simeq \nu_i^{\mathrm{HPCS2,anh}} + \left(\omega_i^{\mathrm{DPCS3,harm}} - \omega_i^{\mathrm{HPCS2,harm}}\right). \tag{5}$$

For nicotinic acid and cyclohexanone, dual-level anharmonic spectra were obtained by combining the HPCS2 GVPT2 transition lists with DPCS3–HPCS2 harmonic corrections in the diagnostic regions. For 1,4-naphthoquinone, the comparison is based on the HPCS2/B3LYP and DPCS3 anharmonic spectra. For cis-1,3,5-hexatriene, HPCS2 and DPCS3 GVPT2 transition lists are compared with the literature vapor-phase assignment and inverse-spectral band analysis.

Direct gas-phase calculated–experimental IR figures are included for molecules with isolated-molecule spectral information: nicotinic acid, cyclohexanone, cis-1,3,5-hexatriene, and 1,4-naphthoquinone. Ascorbic acid is not discussed as a gas-phase IR benchmark because the available IR information is condensed-phase, not an isolated gas-phase spectrum.

2.3. Vitamin-Relevant Motifs and Validation Targets

To benchmark the transferability of PCS-level accuracy to vitamin-relevant motifs, we selected complete vitamin molecules and diagnostic fragments spanning different sizes, rigidities, and functionalization patterns. Nicotinic acid and ascorbic acid represent the complete-vitamin end of this ladder, whereas the other entries isolate structural units that are diagnostic for larger vitamin families. Whenever possible, validation is performed against high-resolution rotational spectra; for compact systems, PCS2 also provides a reference equilibrium geometry. Larger fragments such as 2-decalone and naphthoquinone are deliberately retained because they probe the regime where BDPCS3 must be validated directly against experiment rather than against a PCS2 calculation. The selected systems are therefore a motif validation ladder rather than a disconnected collection of molecules (Table 2).

Table 2. Vitamin-relevant structural motifs and representative systems.

Motif	Representative System	Vitamin Context
Pyridine carboxyl	Nicotinic acid	Vitamin B_3 molecule
Polyhydroxy lactone	Ascorbic acid	Vitamin C molecule
Conjugated polyene	cis-1,3,5-Hexatriene	Minimal model of the vitamin A C9 tetraene side chain
Saturated ketone ring	Cyclohexanone	Vitamin A ring motif
Fused bicyclic ketone	2-Decalone	Vitamin D ring-system proxy
Benzopyran	Isochroman	Vitamin E core motif
Quinone	Naphthoquinone	Vitamin K core motif

Together, these models define a chemically diverse validation ladder. Small fragments test PCS2/BDPCS3 consistency, medium-size systems test direct BDPCS3 transferability, and conformationally rich systems probe the combined sensitivity of equilibrium structures and HPCS2 vibrational corrections.

2.4. Workflow and Validation Strategy

The adaptive protocol is designed to deliver near–spectroscopic accuracy while controlling computational cost. It follows a hierarchical decision process tailored to the chemical diversity of vitamin-relevant fragments:

1. **Direct experimental benchmarking**
   When high-resolution rotational constants are available, geometries are optimized at the DPCS3/BDPCS3 level and converted to ground-state constants with HPCS2 vibrational corrections before comparison with experiment. Agreement near the 0.1% level in rotational constants qualifies the fragment as *validated*; larger deviations are interpreted in terms of conformational flexibility and the quality of the vibrational correction.
2. **High-level theoretical references**
   For compact fragments, PCS2 equilibrium geometries provide an internal reference for assessing the residual BDPCS3 structural error. For larger fragments where PCS2 is not practical, the experimental ground-state rotational constants become the primary validation target after HPCS2 vibrational correction.
3. **Fragment classification**
   A fragment is labeled *validated* if BDPCS3 agrees with experiment or PCS2 at the level required for its

intended use. Flexible, conformationally rich motifs are examined more closely because small residual changes in hydrogen-bond patterns or puckering coordinates can be amplified in the rotational constants.

4. **Treatment of problematic fragments**
   If a motif shows systematic deviations, PCS2—and PCS3 when energetics are critical—is used as a local reference whenever feasible. In larger vitamin assemblies containing such motifs:
   - the **ONIOM** (our own N-layered integrated molecular orbital and molecular mechanics) **(PCS2:BDPCS3)** scheme is applied, restricting high-level treatment to problematic regions; or
   - PCS2–BDPCS3 geometry differences are applied as corrective terms.
5. **Application to larger vitamin targets**
   For a new *Nano-LEGO* target, the molecule is automatically decomposed into chemically meaningful fragments (heteroaromatic cores, polyfunctional linkers, saturated rings, and conjugated units). Fragments represented in the validated library are transferred directly; new motifs are computed at the BDPCS3 level and classified through the same protocol. The same validated library can also be used outside the PCS workflow as a reference set for lower-cost quantum-chemical methods and for force-field parametrization in molecular dynamics.

Vibrational corrections used to convert equilibrium rotational constants to ground-state values are computed at the HPCS2 level, providing a consistent and cost-effective treatment across all fragments.

This combination of model selection, adaptive validation, and fragment-based assembly supports the construction of larger vitamin structures from fragments whose accuracy has been quantified with the same spectroscopic metric (Figure 1).

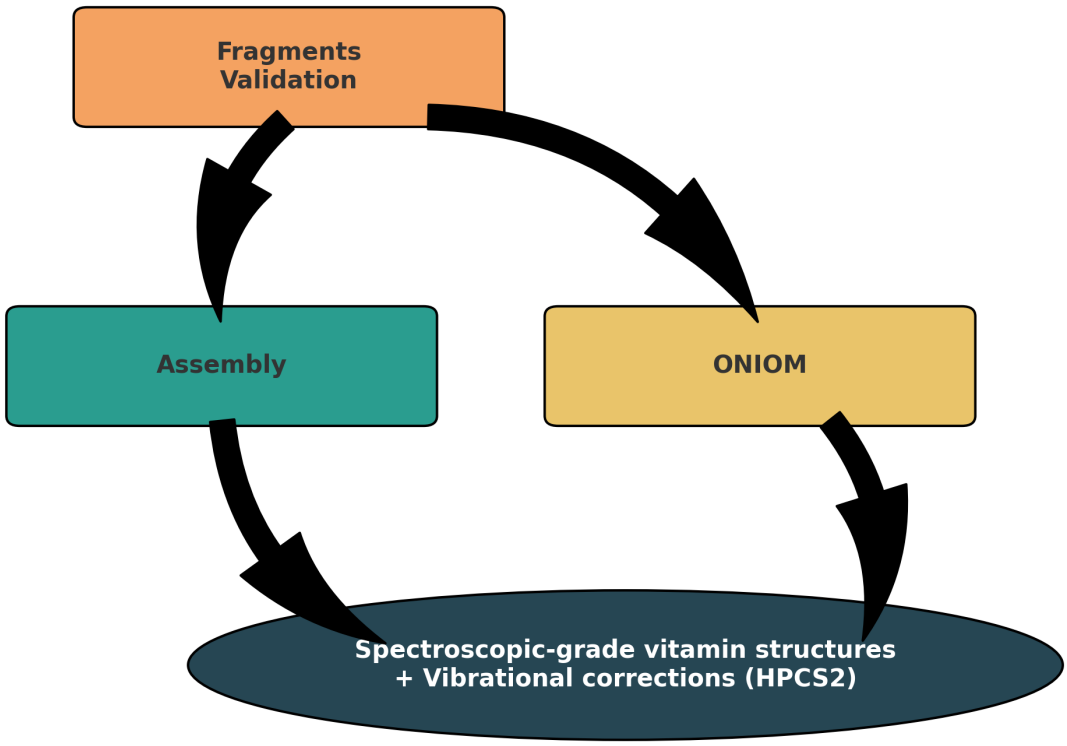

Figure 1. Adaptive fragment-assembly workflow.

3. Results

The reliability of PCS2 reference geometries has been established in recent benchmark studies covering a broad spectrum of ∼150 molecular systems [23]. These investigations report mean unsigned deviations of about 1 mÅ for bond distances and roughly 0.1° for valence angles, which translate into relative errors near 0.1% for rotational constants [14]. In the present work, PCS2 is used whenever molecular size permits, while BDPCS3//HPCS2 is validated directly against experiment for the larger fragments.

In the following tables, Exp. B_0 denotes experimental ground-state rotational constants; computed entries follow the notation defined in the Materials and Methods. The infrared layer provides a second, assignment-oriented check whenever isolated gas-phase spectra or tabulated gas-phase bands are available. This applies to nicotinic acid, cyclohexanone, cis-1,3,5-hexatriene, and 1,4-naphthoquinone. The figures therefore do not attempt a

condensed-phase comparison for vitamin C.

3.1. Nicotinic Acid (Vitamin B_3)

Nicotinic acid is the most compact heteroaromatic benchmark in the set. Two rotamers are observed in the gas phase (Figure 2), and their rotational constants differ by only a few MHz [39], making the system sensitive to small errors in both the pyridine ring and the carboxyl torsion. Table 3 shows that PCS2//HPCS2 and BDPCS3//HPCS2 both reproduce the experimental ground-state constants closely. The residual BDPCS3 deviations are slightly larger for the B and C constants, but remain small enough to validate the pyridine-carboxyl fragment for transfer to vitamin B_3 derivatives.

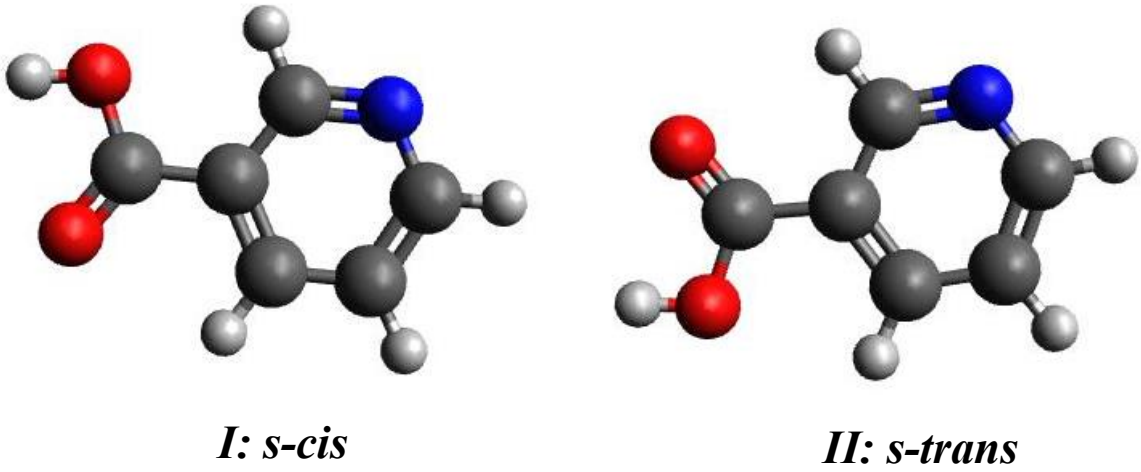

Figure 2. Structures of the two observed nicotinic acid rotamers used as vitamin B_3 fragments.

Table 3. Experimental ground-state constants, equilibrium rotational constants, and HPCS2 vibrational corrections (MHz) for the two observed nicotinic acid rotamers.

Rotamer	Entry	A	B	C
s-cis	Exp. B_0 [a]	3944.2182	1245.13484	947.00712
s-cis	PCS2	3968.8815	1252.1073	951.8246
s-cis	BDPCS3	3973.0398	1251.2377	951.5607
s-cis	HPCS2 ΔB^{vib}	−27.84	−7.77	−5.57
s-cis	PCS2//HPCS2	3941.04	1244.34	946.25
s-cis	BDPCS3//HPCS2	3945.20	1243.47	946.00
s-trans	Exp. B_0 [a]	3947.9594	1243.65955	946.40083
s-trans	PCS2	3972.5246	1250.6790	951.2080
s-trans	BDPCS3	3976.5578	1249.7884	950.9236
s-trans	HPCS2 ΔB^{vib}	−27.71	−7.82	−5.58
s-trans	PCS2//HPCS2	3944.81	1242.86	945.63
s-trans	BDPCS3//HPCS2	3948.85	1242.00	945.34

[a] From Ref. [39]. HPCS2 vibrational corrections are defined as $\Delta B^{vib} = B_0 - B_e$.

The same anharmonic force fields used to compute vibrational corrections to the rotational constants also provide an independent infrared fingerprint for the validated conformer. Figure 3 compares the gas-phase IR spectrum of nicotinic acid with the HPCS2 and DPCS3//HPCS2 anharmonic spectra of conformer I [40]. The fingerprint region is already reproduced well by both calculations, while the carboxylic O–H stretching band provides the clearest distinction between the two models. At the HPCS2 level this band is shifted to lower wavenumber; the dual-level DPCS3//HPCS2 treatment moves it into close agreement with the experimental maximum. The vibrational comparison therefore supports the rotational benchmark: the dual-level protocol improves the local carboxyl description without sacrificing the low-cost anharmonic treatment needed for spectroscopic corrections.

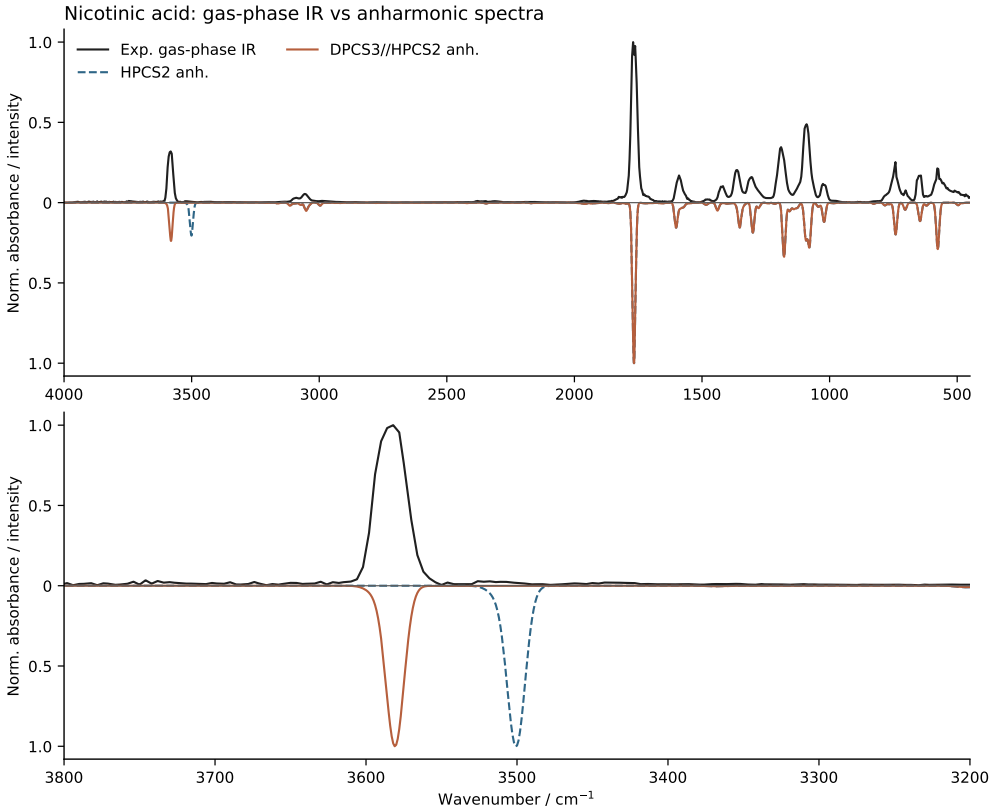

Figure 3. Gas-phase infrared spectrum of nicotinic acid compared with HPCS2 and DPCS3//HPCS2 anharmonic spectra for conformer I. The lower panel shows the carboxylic O–H stretching region.

3.2. Ascorbic Acid (Vitamin C)

Ascorbic acid is the most flexible and strongly hydrogen-bonded benchmark considered here. The lactone ring, enediol unit, and hydroxymethyl substituent generate several competing intramolecular contacts, and the microwave spectrum resolves three conformers with distinct hydrogen-bonding patterns (Figure 4) [2]. This makes vitamin C an intentionally severe structural test: small residual errors in the hydrogen-bond network or ring puckering are amplified in the rotational constants. As expected, the rotational-constant errors are larger than for the more rigid motifs. Nevertheless, the BDPCS3//HPCS2 constants in Table 4 provide the most balanced affordable description, improving substantially over uncorrected equilibrium constants.

The DPCS3 energetics and dipole-moment components in Table 5 further show that the three observed structures are nearly isoenergetic after zero-point correction and have non-negligible principal-axis components. Conformer I is dominated by an a-type component, conformer II has strong a-type and weaker c-type components, and conformer III should support mainly b- and c-type transitions. The coexistence and microwave observability of the three conformers are therefore fully consistent with the computed landscape.

No calculated–experimental gas-phase IR comparison is reported for vitamin C. The available infrared data do not correspond to an isolated gas-phase spectrum, so using them as a direct benchmark would mix intrinsic conformer effects with matrix, crystal, or intermolecular hydrogen-bond shifts.

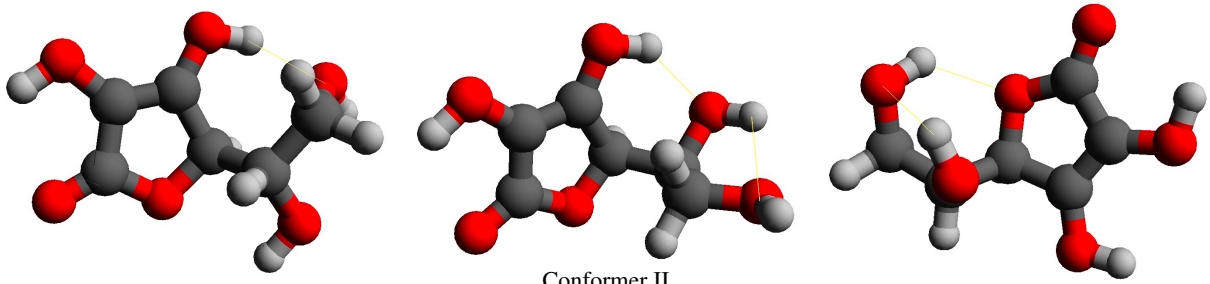

Figure 4. Structures of the three experimentally observed ascorbic acid conformers.

Table 4. Experimental and computed rotational constants (MHz) for the three observed conformers of ascorbic acid.

Conformer	Entry	A	B	C
I	Exp. B_0[a]	1562.4617	715.1478	524.2595
I	HPCS2[b]	1551.7123	711.9422	520.8407
I	DPCS3[b]	1568.2907	717.4868	525.9081
I	BDPCS3[b]	1573.2205	718.4233	526.7955
I	DPCS3//HPCS2[c]	1553.8757	711.7898	521.5661
I	BDPCS3//HPCS2[c]	1558.8055	712.7263	522.4535
II	Exp. B_0[a]	1472.7260	678.0567	575.0076
II	HPCS2[b]	1485.6383	669.7921	568.3333
II	DPCS3[b]	1484.6736	677.4106	575.5455
II	BDPCS3[b]	1484.9116	679.4965	575.7769
II	DPCS3//HPCS2[d]	1463.5396	673.8706	571.5135
II	BDPCS3//HPCS2[d]	1463.7776	675.9565	571.7449
III	Exp. B_0[a]	1455.7136	760.4796	575.4342
III	HPCS2[b]	1439.7310	763.9327	576.6062
III	DPCS3[b]	1457.5573	762.4716	576.5449
III	BDPCS3[b]	1462.7169	762.9851	577.1477
III	DPCS3//HPCS2[e]	1448.7143	754.0456	570.6789
III	BDPCS3//HPCS2[e]	1453.8739	754.5591	571.2817

[a] From Ref. [2]; conformers I, II, and III correspond to the reported (1,3,6,8), (1,5,7), and (1,2,4,7) hydrogen-bonding patterns. [b] Uncorrected equilibrium constants. [c] Equilibrium constants plus conformer-I HPCS2 vibrational corrections $\Delta B^{vib} = B_0 - B_e = (-14.415, -5.697, -4.342)$ MHz. [d] Equilibrium constants plus conformer-II HPCS2 vibrational corrections $\Delta B^{vib} = (-21.134, -3.540, -4.032)$ MHz. [e] Equilibrium constants plus conformer-III HPCS2 vibrational corrections $\Delta B^{vib} = (-8.843, -8.426, -5.866)$ MHz.

Table 5. DPCS3 relative stabilities and principal-axis dipole-moment components for the three observed ascorbic acid conformers.

Conformer	ΔE_{el}	Δ_{ZPE} kcal mol^{-1}	$\Delta(E_{\mathrm{el}} + E_{\mathrm{ZPE}})$	(μ_a, μ_b, μ_c) D
I	0.00	0.00	0.00	(3.667, −0.248, −0.029)
II	0.47	−0.27	0.20	(3.779, 0.262, 1.116)
III	0.39	−0.26	0.13	(0.529, −2.794, −1.736)

Relative electronic energies are from DPCS3 total energies; Δ_{ZPE} values are HPCS2 anharmonic zero-point energy differences with conformer I as reference.

3.3. Vitamin A/D Ring and Polyene Motifs

The vitamin A/D subset probes three complementary structural motifs (Figure 5): a puckered saturated ring (cyclohexanone), a minimal conjugated polyene segment (cis-1,3,5-hexatriene), and a fused bicyclic ketone (2-decalone). Cyclohexanone provides the most direct comparison because PCS2, DPCS3, and BDPCS3 can all be tested after applying the same vibrational correction to the ground-state constants. BDPCS3//HPCS2 gives the smallest residual deviations among the affordable models, with unsigned relative errors of only about 0.04–0.06%, whereas DPCS3//HPCS2 remains less accurate (Table 6).

The larger 2-decalone conformers require a different treatment: PCS2 is no longer a practical reference, so validation is performed directly by comparing BDPCS3//HPCS2 ground-state constants with experiment. The agreement is particularly good for the trans conformer and remains within the expected accuracy range for the two cis forms, whose different puckering patterns provide a demanding test of fused-ring transferability. The same calculations give a consistent conformational picture (Table 7): trans is lowest in energy, while cis-S and cis-NS lie 2.49 and 2.63 kcal mol^{-1} higher after zero-point correction. The principal-axis dipole components indicate multiple allowed transition types for each conformer, supporting their microwave detectability. The cis-hexatriene data in Table 8 provide a limiting vitamin A proxy by testing the smallest experimentally characterized segment that retains the conjugated-chain vibrational pattern.

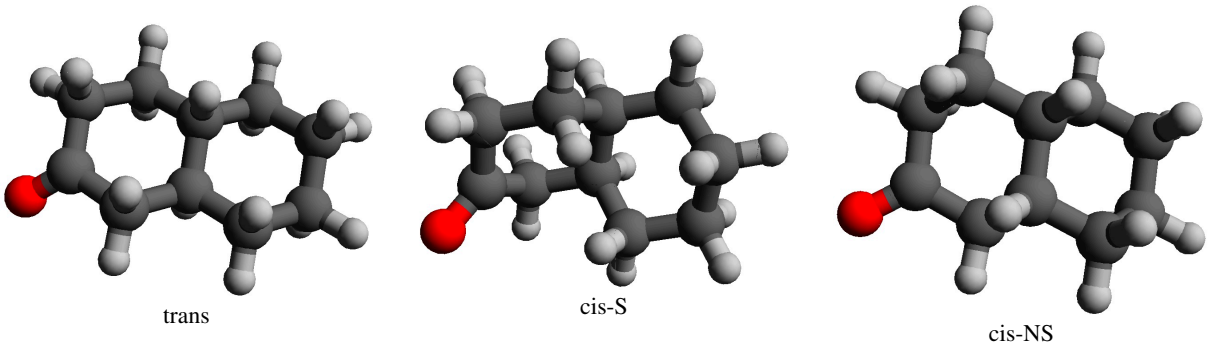

Figure 5. Structures of the three experimentally observed 2-decalone conformers.

Table 6. Rotational constants (MHz) for vitamin-relevant ring motifs.

System	Entry	A	B	C
Cyclohexanone[a]	Exp. B_0	4195.3	2502.6	1754.4
Cyclohexanone[a]	DPCS3	4203.7	2519.6	1769.0
Cyclohexanone[a]	BDPCS3	4220.0	2529.6	1775.6
Cyclohexanone[a]	PCS2	4226.0	2530.7	1776.8
Cyclohexanone[a]	HPCS2 ΔB^{vib}	−26.4	−27.9	−22.2
Cyclohexanone[a]	DPCS3//HPCS2	4177.3	2491.7	1746.8
Cyclohexanone[a]	BDPCS3//HPCS2	4193.6	2501.7	1753.4
Cyclohexanone[a]	PCS2//HPCS2	4199.6	2502.8	1754.6
2-Decalone trans[b]	Exp. B_0	2229.28469	757.765892	604.276175
2-Decalone trans[b]	DPCS3	2235.9153	762.6322	608.7241
2-Decalone trans[b]	BDPCS3	2245.6982	765.1597	610.8164
2-Decalone trans[b]	HPCS2 ΔB^{vib}	−16.073	−8.203	−7.055
2-Decalone trans[b]	DPCS3//HPCS2	2219.8423	754.4292	601.6691
2-Decalone trans[b]	BDPCS3//HPCS2	2229.6252	756.9567	603.7614
2-Decalone cis-S[b]	Exp. B_0	1992.82844	853.595752	726.007720
2-Decalone cis-S[b]	DPCS3	1998.1016	860.3124	731.9235
2-Decalone cis-S[b]	BDPCS3	2007.6981	862.4433	733.5758
2-Decalone cis-S[b]	HPCS2 ΔB^{vib}	−9.734	−11.693	−10.078
2-Decalone cis-S[b]	DPCS3//HPCS2	1988.3676	848.6194	721.8455
2-Decalone cis-S[b]	BDPCS3//HPCS2	1997.9641	850.7503	723.4978
2-Decalone cis-NS[b]	Exp. B_0	1990.2260	847.214331	696.886991
2-Decalone cis-NS[b]	DPCS3	2006.1822	851.9195	700.1248
2-Decalone cis-NS[b]	BDPCS3	2016.2353	854.0777	701.9266
2-Decalone cis-NS[b]	HPCS2 ΔB^{vib}	−23.088	−8.697	−6.737
2-Decalone cis-NS[b]	DPCS3//HPCS2	1983.0942	843.2225	693.3878
2-Decalone cis-NS[b]	BDPCS3//HPCS2	1993.1473	845.3807	695.1896

[a] Cyclohexanone experimental ground-state constants are from Ref. [41]. [b] From Ref. [42]. Vibrational corrections are defined as $\Delta B^{vib} = B_0 - B_e$; model//HPCS2 ground-state constants are obtained as $B_e + \Delta B^{vib}$.

The gas-phase IR spectrum of cyclohexanone adds a local force-field check for the saturated ketone motif (Figure 6). The dominant experimental carbonyl envelope is centered near 1734 cm^{-1} in the JCAMP-DX trace. The HPCS2 anharmonic spectrum places the main carbonyl intensity above the experimental envelope, whereas the DPCS3//HPCS2 dual-level spectrum shifts the carbonyl feature toward the observed maximum and preserves the C–H and fingerprint-region envelopes. The IR data therefore support the same conclusion as the rotational constants: cyclohexanone is a reliable transferable saturated-ring carbonyl motif, with the residual vibrational error concentrated mainly in the carbonyl stretching position.

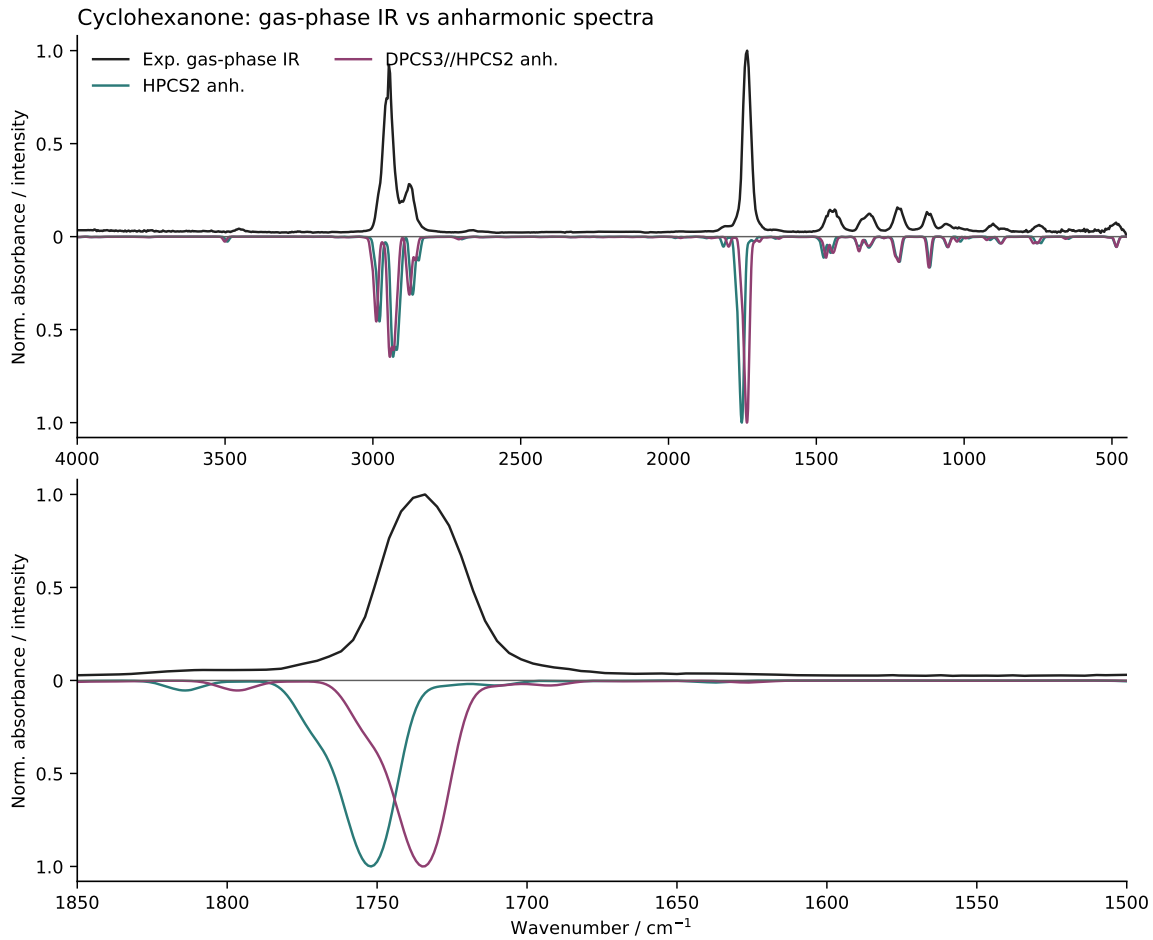

Figure 6. Gas-phase infrared spectrum of cyclohexanone compared with HPCS2 and DPCS3//HPCS2 anharmonic spectra. The lower panel shows the carbonyl-stretching region.

Table 7. Relative stabilities and DPCS3 principal-axis dipole-moment components for the 2-decalone conformers.

Conformer	ΔE_{el}	Δ_{ZPE} kcal mol^{-1}	$\Delta(E_{\mathrm{el}}+E_{\mathrm{ZPE}})$	(μ_a,μ_b,μ_c) D
trans	0.00	0.00	0.00	(3.062, 1.137, 1.212)
cis-S	2.17	0.32	2.49	(−2.601, 1.458, 1.532)
cis-NS	2.41	0.22	2.63	(3.181, 1.487, 0.052)

Relative electronic energies are from DPCS3 total energies; Δ_{ZPE} values are HPCS2 anharmonic zero-point energy differences with trans as reference.

Table 8. Experimental ground-state constants, equilibrium rotational constants, and HPCS2 vibrational corrections (MHz) for cis-1,3,5-hexatriene, the minimal polyene fragment for vitamin A.

Entry	A	B	C
Exp. B_0 [a]	14651.229	1583.851	1429.461
PCS2	14790.1652	1591.0107	1436.4849
HPCS2	14876.0343	1565.8299	1416.7092
HPCS2 ΔB^{vib}	−160.0	−8.0	−7.5
PCS2//HPCS2	14630.1652	1583.0107	1428.9849
DPCS3	14805.9256	1584.3378	1431.1904
BDPCS3	14864.2130	1586.2278	1433.2763
DPCS3//HPCS2	14645.9256	1576.3378	1423.6904
BDPCS3//HPCS2	14704.2130	1578.2278	1425.7763

[a] From Ref. [43]. PCS2//HPCS2 gives mean and maximum unsigned relative deviations of 0.077% and 0.144%, respectively, compared with 0.305% and 0.474% for DPCS3//HPCS2 and 0.325% and 0.362% for BDPCS3//HPCS2. This behavior contrasts with the generally similar PCS2//HPCS2 and BDPCS3//HPCS2 performance found for the other compact benchmarks, and is consistent with the higher sensitivity of carotenoid-like alternating single-/double-bond chains to residual DFT-based structural errors.

The IR spectrum of cis-1,3,5-hexatriene provides the complementary vibrational check for the vitamin A polyene motif (Figure 7). This molecule is intentionally a minimal model, not a direct surrogate for retinol: cis-1,3,5-hexatriene is a C6 triene, whereas the retinoid side chain is a C9 tetraene conjugated with the β-ionone double bond to form an extended pentaene chromophore. It therefore isolates the shortest experimentally accessible segment of the conjugated-chain force field in a gas-phase system for which microwave and vapor-phase vibrational information are available.

The historical vapor- and liquid-phase study established the cis assignment from the number of IR/Raman coincidences and the observed band contours [44], while the later inverse-spectral analysis reported experimental band positions, intensities, and half-widths suitable for quantitative envelope comparison [45]. The HPCS2 and DPCS3 anharmonic spectra reproduce the diagnostic polyene pattern, including the intense out-of-plane and in-plane fingerprint bands near 980–900 cm^{-1} and the C–H stretching envelope above 3000 cm^{-1}. The remaining discrepancies mainly involve intensity redistribution among closely spaced modes, as expected for a conjugated chain in which electrical anharmonicity and band overlap strongly influence the apparent envelope. The rotational and IR evidence are therefore consistent: cis-hexatriene is a transferable minimal polyene fragment, but its IR validation should be read as an assignment-pattern test rather than as an isolated single-band benchmark.

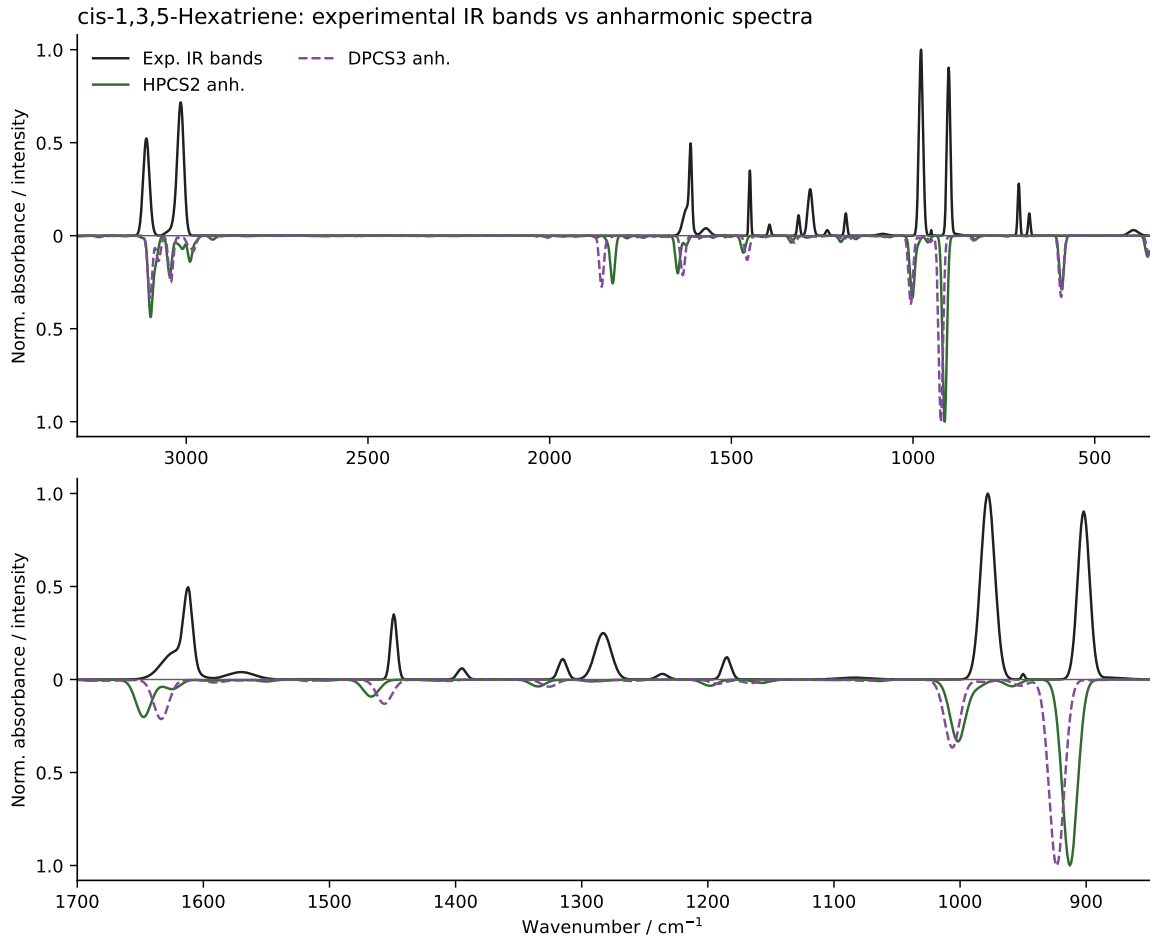

Figure 7. Experimental infrared band envelope of cis-1,3,5-hexatriene compared with HPCS2 and DPCS3 anharmonic spectra. The lower panel shows the polyene fingerprint region.

3.4. Isochroman (Vitamin E Benzopyran Motif)

Isochroman is a benzopyran fragment for vitamin E and provides one of the cleanest rotational validation cases considered here. The PCS2//HPCS2 and BDPCS3//HPCS2 ground-state constants in Table 9 are both very close to the experimental microwave constants of the observed conformer. BDPCS3//HPCS2 reproduces the experimental A, B, and C constants within about 1.2, 0.4, and 0.2 MHz, respectively, supporting transfer of the benzopyran fragment to larger tocopherol-like structures.

This structural role is also supported by the vibrational study of Navarro and co-workers [3], who selected isochroman as the first component in a sequential analysis of tocopherols and tocotrienols, recorded vapor, liquid, and solution IR spectra, and explicitly related the benzopyran nucleus to the full vitamin E families. Isochroman is

therefore treated as a rotationally validated vitamin E motif with literature vibrational support; it is the only motif in the present set for which a matched PCS-level calculated–experimental IR figure is not included.

Table 9. Experimental ground-state constants, equilibrium constants, and HPCS2 vibrational corrections (MHz) for isochroman.

Entry	A	B	C
Exp. B_0 [a]	2892.7434	1140.4878	842.9092
PCS2	2915.1865	1147.7491	848.3313
DPCS3	2906.2112	1143.8031	845.3581
BDPCS3	2916.1629	1147.5420	848.1128
HPCS2 ΔB^{vib}	−24.61	−7.41	−5.37
PCS2//HPCS2	2890.5765	1140.3391	842.9613
DPCS3//HPCS2	2881.6012	1136.3931	839.9881
BDPCS3//HPCS2	2891.5529	1140.1320	842.7428

[a] From Ref. [46].

3.5. Naphthoquinone (Core Scaffold of Vitamin K)

Quinone derivatives test the conjugated carbonyl/aromatic region of the model space. Benzoquinone is used as a compact PCS2 benchmark for the local quinone geometry; an experimental dipole-allowed rotational spectrum is not expected for the isolated molecule because its dipole moment is zero. Naphthoquinone then extends the same motif to the core scaffold of vitamin K. Because it is beyond the convenient PCS2 range, its validation relies on direct comparison of BDPCS3//HPCS2 ground-state constants with experiment. Tables 10 and 11 show that both the local quinone geometry and the global moments of inertia are reproduced well, supporting transfer of the quinone fragment to larger vitamin K analogues.

Table 10. Selected bond lengths (Å) and bond angles (degrees) for the benzoquinone model optimized at the PCS2 and BDPCS3 levels.

Parameter	PCS2	BDPCS3
C=O (quinone)	1.2201	1.2202
C-C (ring)	1.4793	1.4795
O-C-C angle	121.28	121.29

Table 11. Rotational constants (MHz) for benzoquinone (BQ) and naphthoquinone (NQ).

System	Entry	A	B	C
BQ	PCS2	5272.1	1667.9	1267.1
BQ	BDPCS3	5271.5	1667.9	1267.0
NQ	BDPCS3	1333.7	1100.1	602.9
NQ	BDPCS3//HPCS2[a]	1327.3	1092.5	599.6
NQ	Exp.[b]	1328.3	1092.8	599.9

[a] Obtained from BDPCS3 equilibrium constants using HPCS2 $\Delta B^{vib} = (-6.4, -7.6, -3.3)$ MHz. [b] Experimental ground-state constants from Ref. [47]; the same HPCS2 corrections were removed from the reported semi-experimental values.

The gas-phase IR trace of 1,4-naphthoquinone provides a complementary test of the quinone force field (Figure 8). The figure compares the experiment with the HPCS2 and DPCS3 anharmonic spectra. The strongest experimental bands occur in the quinone carbonyl region near 1682 cm^{-1} and in the fingerprint region near 1294 and 762 cm^{-1}; these features are also the most diagnostic parts of the calculated spectra.

This fragment is directly connected to vitamin K chemistry: menadione (vitamin K_3) is 2-methyl-1,4-naphthoquinone, and recent mid-infrared/near-infrared work on crystalline menadione explicitly analyzes the naphthoquinone moiety and its carbonyl and ring-mode pattern [4]. Together with the rotational constants, the gas-phase 1,4-naphthoquinone spectrum therefore validates the parent quinone core of vitamin K, while identifying methyl substitution as the next structural refinement needed for full menadione.

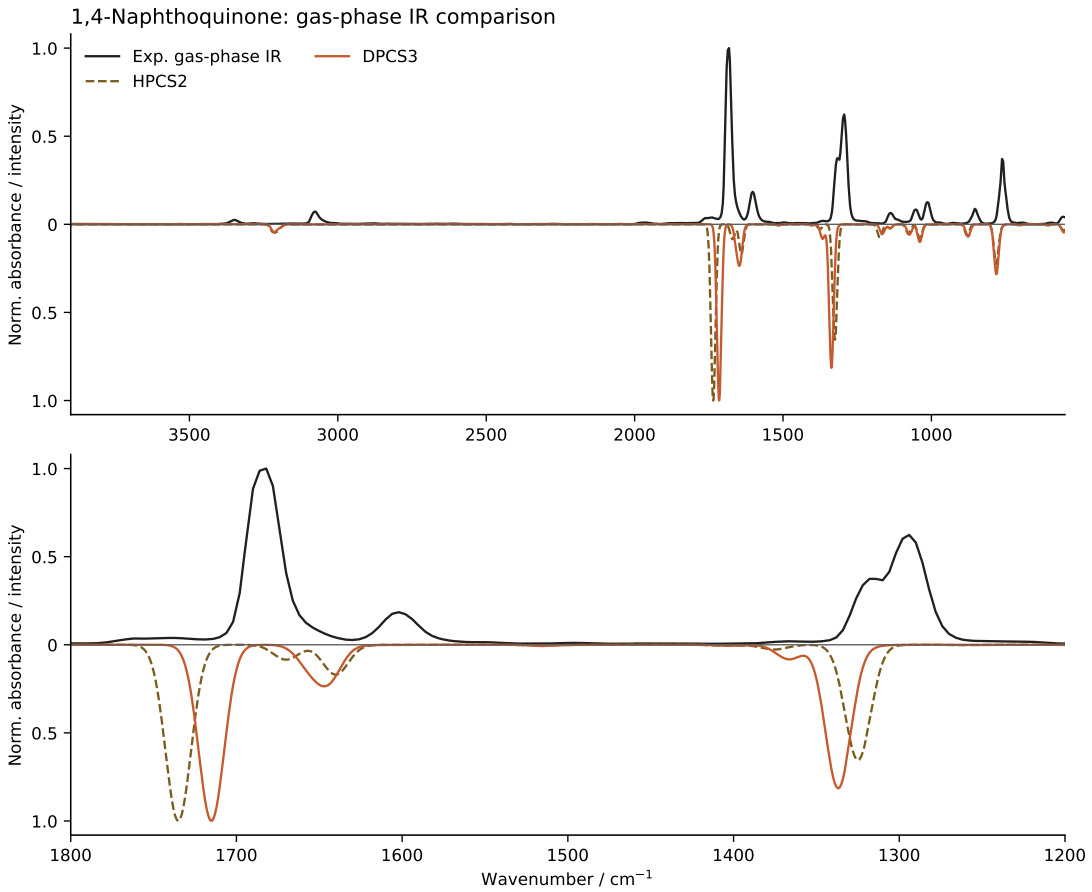

Figure 8. Gas-phase infrared spectrum of 1,4-naphthoquinone compared with HPCS2 and DPCS3 anharmonic spectra. The lower panel shows the quinone carbonyl and ring-stretching region.

4. Discussion

The numerical results support the reference-to-transfer strategy outlined in the Introduction. Once equilibrium structures are converted to ground-state constants with HPCS2 vibrational corrections, BDPCS3 reproduces the experimental rotational constants of several transferable motifs at or near the target accuracy. The global statistics in Table 12 quantify this behavior: the complete benchmark gives a mean unsigned deviation of 0.213%, while the non-H-bonded subset gives a mean unsigned deviation of 0.135%, with no individual constant in that subset deviating by more than 0.362%. These figures are consistent with earlier large-scale PCS/Nano-LEGO statistics, which showed that bond-corrected composite structures typically reduce rotational-constant errors by about a factor of three to five relative to methods of comparable cost [28,29].

The informative cases are the chemically expected deviations. In compact systems for which both levels are practical, PCS2//HPCS2 and BDPCS3//HPCS2 usually give comparable ground-state rotational constants. The clear exception is cis-1,3,5-hexatriene: PCS2//HPCS2 is substantially closer to experiment than the DFT-based DPCS3//HPCS2 and BDPCS3//HPCS2 values, indicating that carotenoid-like polyene chains remain difficult because bond-length alternation directly controls the moments of inertia. Larger or more conformationally sensitive systems, notably 2-decalone and ascorbic acid, expose different limits: the structural model remains useful, but residual errors increase when ring puckering or hydrogen-bond patterns strongly affect the rotational constants. This distinction is essential for the adaptive workflow because it identifies which fragments can be transferred directly and which require local refinement or explicit uncertainty margins.

The IR layer asks a complementary question: whether structures that pass the rotational test also generate chemically recognizable local fingerprints. Nicotinic acid shows how a local dual-level correction improves the carboxylic O–H stretching region, cyclohexanone tests the carbonyl and C–H envelopes of a saturated ketone ring, cis-hexatriene probes the conjugated polyene fingerprint, and naphthoquinone verifies the quinone carbonyl/ring pattern through a direct calculated–experimental spectral comparison. The diagnostic band statistics in Table 13 keep this comparison quantitative: the mean unsigned band-position errors remain between 7.6 and 29.3 cm^{-1} across the IR validation subset. These spectra do not replace rotational constants as structural benchmarks; they test the local force-field layer that rotational constants alone cannot isolate.

The smaller IR error for nicotinic acid has a specific spectroscopic origin and should not be interpreted as uniformly higher accuracy for every vibrational coordinate. At the HPCS2 level, the carboxylic O–H stretching maximum is displaced by about 80 cm^{-1}, whereas the DPCS3//HPCS2 dual-level correction shifts this isolated and highly diagnostic band into near coincidence with experiment. The remaining nicotinic-acid fingerprint maxima have unsigned deviations of 4–12 cm^{-1}, so the low mean in Table 13 reflects both the successful local repair of the O–H stretch and the relatively sparse spectrum of this compact heteroaromatic acid.

The larger averages for cyclohexanone, cis-hexatriene, and naphthoquinone arise mainly from congested C–H, polyene, quinone, and fingerprint envelopes, where several close-lying modes redistribute intensity and the experimental maximum represents an apparent band centre rather than a single isolated transition. The IR statistics should therefore be read together with the assignments and spectral envelopes, not as a single global ranking of force-field quality. In that sense, cyclohexanone and naphthoquinone can show accurate carbonyl positions while still retaining larger mean errors in their diagnostic statistics.

Table 12. Global error statistics for the vitamin-relevant motifs.

System	N	Mean (%)	Max (%)
Nicotinic acid	6	0.090	0.134
Ascorbic acid	9	0.448	0.779
Cyclohexanone	3	0.044	0.057
cis-1,3,5-Hexatriene	3	0.325	0.362
2-Decalone	9	0.195	0.346
Isochroman	3	0.031	0.041
Naphthoquinone	3	0.051	0.075
All systems	36	0.213	0.779
Non-H-bonded motifs	27	0.135	0.362

N is the number of rotational constants included in each statistic. All deviations are evaluated against experimental ground-state constants, Exp. B_0. Mean and Max are the mean and maximum unsigned relative deviations, in percent, over the A, B, and C rotational constants and over all conformers reported for each system. Aggregate rows are computed over the corresponding individual constants, not as averages of the system rows. The final validation level is BDPCS3//HPCS2 for ground-state comparisons.

Table 13. Band-position errors for diagnostic infrared maxima.

System	Diagnostic bands	Spectrum	N	Mean cm^{-1}	Max cm^{-1}
Nicotinic acid	O–H/carboxyl/fingerprint	DPCS3//HPCS2 anh.	5	7.6	12.0
Cyclohexanone	C=O/C–H/fingerprint	DPCS3//HPCS2 anh.	7	17.7	45.0
cis-1,3,5-Hexatriene	C–H/polyene fingerprint	DPCS3 anh.	8	19.6	35.0
1,4-Naphthoquinone	C=O/ring/fingerprint	DPCS3 anh.	6	29.3	45.0

Mean and Max are unsigned band-centre deviations from experiment over the selected diagnostic maxima. The maxima were extracted from the normalized broadened profiles used in Figures 3–8.

5. Conclusions

This work establishes an integrated rotational–infrared validation ladder for PCS models of vitamin-relevant molecular motifs. The benchmark is deliberately gas-phase and multispectroscopic: rotational constants test the global mass distribution and provide quantitative structural error statistics, whereas IR spectra test the local force fields and diagnostic vibrational fingerprints generated by the same structures. This combination is essential for transferable vitamin building blocks, where a geometry can reproduce moments of inertia accurately yet still fail in chemically decisive carbonyl, polyene, quinone, or hydrogen-bond-sensitive regions.

By removing solvent, matrix, packing, and host–guest perturbations, the comparisons isolate the intrinsic geometries and force fields that more complex simulations must recover before environmental effects are added. The present data are therefore not an alternative to condensed-phase or biological modeling. They define a reference layer against which such models, lower-cost quantum-chemical methods, and molecular-dynamics force fields can be calibrated.

Across the complete set, BDPCS3 equilibrium structures combined with HPCS2 vibrational corrections provide a reliable route to experimental ground-state rotational constants. Compact fragments benefit from the PCS2 reference, while larger systems such as 2-decalone and naphthoquinone demonstrate that BDPCS3//HPCS2

can be validated directly against experiment when PCS2 optimizations are no longer practical. The rotational benchmark gives a mean unsigned deviation of 0.213% over all systems and 0.135% for the non-hydrogen-bonded subset, confirming that the accuracy trends previously observed in broad PCS/Nano-LEGO studies extend to vitamin-derived motifs [28,29].

The IR comparisons refine this structural classification. Nicotinic acid validates the heteroaromatic carboxyl motif through both rotational constants and the O–H/carboxyl fingerprint; cyclohexanone validates the saturated ketone ring through its carbonyl and C–H envelopes; cis-hexatriene validates the minimal conjugated polyene band pattern relevant to vitamin A; and 1,4-naphthoquinone validates the quinone carbonyl/ring fingerprint of the vitamin K core through a direct spectral comparison, with menadione corresponding to methyl substitution on this scaffold. Isochroman is the deliberate exception to the full rotational-plus-IR protocol: it is supported by microwave validation and by prior vapor-phase vibrational work connecting the benzopyran nucleus to tocopherols and tocotrienols, but it is not assigned a new PCS-level calculated–experimental IR figure here. Vitamin C remains a structural rotational benchmark but is not used as an IR benchmark because no isolated gas-phase spectrum is available.

The outcome is a transferability map rather than a single-method ranking. Nicotinic acid, cyclohexanone, cis-1,3,5-hexatriene, isochroman, and naphthoquinone emerge as validated building blocks with small residual uncertainty. Ascorbic acid and delicate fused-ring motifs define the regime where hydrogen bonding and puckering require local refinement or explicit uncertainty margins. In the *Nano-LEGO* perspective, high-level accuracy can be assigned to the fragments that control each observable, while larger vitamin architectures are assembled from components whose rotational and vibrational limits have been quantified.

Overall, the PCS/BDPCS3/HPCS2 workflow, combined with GVPT2 anharmonic corrections rather than a routine RRHO treatment, provides a scalable route to spectroscopically reliable structures of complex natural products. By requiring consistency between rotational constants and IR fingerprints wherever matched gas-phase data are available, the present set of vitamin-relevant building blocks establishes a more stringent foundation for future fragment-based modeling than either observable could provide alone.

Supplementary Materials

The additional data and information can be downloaded at: https://media.sciltp.com/articles/others/260716 1352296160/PS-26060010-SM.pdf. The supplementary file contains Cartesian coordinates, rotational constants, vibrational corrections, and auxiliary conformer data for the optimized structures. The same data will be made freely available through the LCB25 database.

Funding

This work was supported by a Research and Development grant from Gaussian Inc.

Institutional Review Board Statement

Not applicable.

Informed Consent Statement

Not applicable.

Data Availability Statement

The structural, rotational, vibrational, and infrared data generated and analyzed in this work will be made available through the LCB25 database at https://www.skies-village.it/webtools/Databases/LCB25/index.html.

Conflicts of Interest

The author declares no competing financial interests beyond the disclosed Research and Development grant from Gaussian Inc.

Use of AI and AI-Assisted Technologies

No AI tools were utilized for this paper.

References

1. Uriarte, I.; Melandri, S.; Maris, A.; et al. Shapes, Dynamics, and Stability of β-Ionone and Its Two Mutants Evidenced by High-Resolution Spectroscopy in the Gas Phase. *J. Phys. Chem. Lett.* **2018**, *9*, 1497–1502. https://doi.org/10.1021/acs.jpclett.8b00256.
2. Peña, I.; Daly, A.M.; Cabezas, C.; et al. Disentangling the Puzzle of Hydrogen Bonding in Vitamin C. *J. Phys. Chem. Lett.* **2013**, *4*, 65–69. https://doi.org/10.1021/jz301947g.
3. Navarro, A.; López González, J.J.; García Fernández, A.; et al. Structural and Vibrational Study of Isochroman. *Chem. Phys.* **2005**, *313*, 279–291. https://doi.org/10.1016/j.chemphys.2005.01.014.
4. Beć, K.B.; Grabska, J.; Huck, C.W.; et al. Anharmonicity and Spectra–Structure Correlations in MIR and NIR Spectra of Crystalline Menadione (Vitamin K3). *Molecules* **2021**, *26*, 6779. https://doi.org/10.3390/molecules26226779.
5. Alonso, J.L.; López, J.C. Microwave Spectroscopy of Biomolecular Building Blocks. In *Gas-Phase IR Spectroscopy and Structure of Biological Molecules*; Springer: Berlin/Heidelberg, Germany, 2015; Volume 364, pp. 335–401. https://doi.org/10.1007/128_2014_601.
6. Domingos, S.R.; Pérez, C.; Schnell, M. Sensing Chirality with Rotational Spectroscopy. *Annu. Rev. Phys. Chem.* **2018**, *69*, 499–519. https://doi.org/10.1146/annurev-physchem-052516-050629.
7. Loru, D.; Sun, W.; Gougoula, E.; et al. Structure and Dynamics of Microhydrated Complexes Revealed with Rotational Spectroscopy. *Annu. Rev. Phys. Chem.* **2026**, *77*, 397–416. https://doi.org/10.1146/annurev-physchem-082324-102016.
8. Rijs, A.M.; Oomens, J. (Eds.) *Gas-Phase IR Spectroscopy and Structure of Biological Molecules*; Topics in Current Chemistry; Springer International Publishing: Cham, Switzerland, 2015; Volume 364.
9. Bakels, S.; Gaigeot, M.P.; Rijs, A.M. Gas-Phase Infrared Spectroscopy of Neutral Peptides: Insights from the Far-IR and THz Domain. *Chem. Rev.* **2020**, *120*, 3233–3260. https://doi.org/10.1021/acs.chemrev.9b00547.
10. Fausto, R.; Borba, A.; Gómez-Zavaglia, A. Light Induced Reactions in Cryogenic Matrices (Highlights 2013–2014). In *Photochemistry*; Fasani, E.; Albini, A., Eds.; The Royal Society of Chemistry: Cambridge, UK, 2015; Volume 43, pp. 20–82.
11. Magyarfalvi, G.; Tarczay, G.; Vass, E. Vibrational Circular Dichroism. *WIREs Comput. Mol. Sci.* **2011**, *1*, 403–425. https://doi.org/10.1002/wcms.39.
12. Demaison, J.; Boggs, J.E.; Császár, A.G. (Eds.) *Equilibrium Molecular Structures: From Spectroscopy to Quantum Chemistry*; CRC Press: Boca Raton, FL, USA, 2011.
13. Puzzarini, C.; Stanton, J.F.; Gauss, J. Quantum-Chemical Calculation of Spectroscopic Parameters for Rotational Spectroscopy. *Int. Rev. Phys. Chem.* **2010**, *29*, 273–367.
14. Puzzarini, C.; Stanton, J.F. Connections Between the Accuracy of Rotational Constants and Equilibrium Molecular Structures. *Phys. Chem. Chem. Phys.* **2023**, *25*, 1421–1429.
15. Pulay, P.; Meyer, W.; Boggs, J.E. Cubic Force Constants and Equilibrium Geometry of Methane From Hartree–Fock and Correlated Wavefunctions. *J. Chem. Phys.* **1978**, *68*, 5077–5085.
16. Mendolicchio, M.; Barone, V. Unbiased Comparison Between Theoretical and Experimental Molecular Structures and Properties: Toward an Accurate Reduced-Cost Evaluation of Vibrational Contributions. *J. Chem. Theory Comput.* **2024**, *20*, 2842–2857.
17. Mendolicchio, M.; Barone, V. Accurate Vibrational and Ro-vibrational Contributions to the Properties of Large Molecules by a New Engine Employing Curvilinear Internal Coordinates and Vibrational Perturbation Theory to Second Order. *J. Chem. Theory Comput.* **2024**, *20*, 8378–8395.
18. Barone, V.; Di Grande, S.; Puzzarini, C. Gas-phase computational spectroscopy: the challenge of the molecular bricks of life. *Ann. Rev. Phys. Chem.* **2023**, *74*, 29–52.
19. Barone, V. Quantum Chemistry Meets High-Resolution Spectroscopy for Characterizing the Molecular Bricks of Life in the Gas-Phase. *Phys. Chem. Chem. Phys.* **2024**, *26*, 5802–5821.
20. Barone, V.; Di Grande, S.; Puzzarini, C. Toward Accurate yet Effective Computations of Rotational Spectroscopic Parameters for Biomolecule Building Blocks. *Molecules* **2023**, *28*, 913.
21. Barone, V.; Fusè, M.; Lazzari, F.; et al. Benchmark Structures and Conformational Landscapes of Amino Acids in the Gas Phase: a Joint Venture of Machine Learning, Quantum Chemistry, and Rotational Spectroscopy. *J. Chem. Theory Comput.* **2023**, *19*, 1243–1260.
22. Barone, V. From Perception to Prediction and Interpretation: Enlightening the Gray Zone of Molecular Bricks of Life with the Help of Machine Learning and Quantum Chemistry. *WIREs Comput. Mol. Sci.* **2025**, *15*, e70000.
23. Di Grande, S.; Barone, V. Toward Accurate Quantum Chemical Methods for Molecules of Increasing Dimension: the New Family of Pisa Composite Schemes. *J. Phys. Chem. A* **2024**, *128*, 4886–4900.
24. Crisci, L.; Lazzari, F.; Barone, V. Composite Gradient Schemes for Accurate Molecular Geometries: A Flexible Interface and Hierarchical Optimization Workflow. *J. Phys. Chem. Lett.* **2025**, *16*, 7376–7382.
25. Crisci, L.; Lazzari, F.; Barone, V. Accurate, Affordable and Unsupervised: Analytical F12 Gradients Driven by Generalized Internal Coordinates. *J. Phys. Chem. Lett.* **2025**, *16*, 9985–9992.
26. Barone, V. PCS/Bonds: Pick your Molecule and Get Its Accurate Structure and Rotational Constants at DFT Cost. *J. Chem. Phys.* **2023**, *159*, 081102.

27. Mendolicchio, M.; Uribe, L.; Lazzari, F.; et al. Computational Efficiency Meets Spectroscopic Accuracy: An Unsupervised Workflow for Equilibrium Geometries and Vibrational Effects in Gas-Phase Prebiotic Molecules. *Phys. Chem. Chem. Phys.* **2025**, *27*, 16383–16397.
28. Barone, V.; Crisci, L.; Lazzari, F. The Road to Affordable Accuracy beyond Small Molecules: From Energetics toward Molecular Structure. *Acc. Chem. Res.* **2026**, *59*, 270–284. https://doi.org/10.1021/acs.accounts.5c00718.
29. Barone, V.; Ceselin, G.; Lazzari, F.; et al. Toward Spectroscopic Accuracy for the Structures of Large Molecules at DFT Cost: Refinement and Extension of the Nano-LEGO Approach. *J. Phys. Chem. A* **2023**, *127*, 5183–5192.
30. Peterson, K.A.; Adler, T.B.; Werner, H.J. Systematically Convergent Basis Sets for Explicitly Correlated Wavefunctions: The Atoms H, He, B–Ne, and Al–Ar. *J. Chem. Phys.* **2008**, *128*, 084102.
31. Peterson, K.A.; Dunning Jr., T.H. Accurate Correlation Consistent Basis Sets for Molecular Core–Valence Correlation Effects: The Second Row Atoms Al–Ar, and the First Row Atoms B–Ne Revisited. *J. Chem. Phys.* **2002**, *117*, 10548–10560.
32. Yousaf, K.E.; Peterson, K.A. Optimized Auxiliary Basis Sets For Explicitly Correlated Methods. *J. Chem. Phys.* **2008**, *129*, 184108.
33. Yousaf, K.E.; Peterson, K.A. Optimized Complementary Auxiliary Basis Sets For Explicitly Correlated Methods: aug-cc-pVnZ Orbital Basis Sets. *Chem. Phys. Lett.* **2009**, *476*, 303–307.
34. Santra, G.; Sylvetsky, N.; Martin, J.M. Minimally Empirical Double-Hybrid Functionals Trained Against the GMTKN55 Database. *J. Phys. Chem. A* **2019**, *123*, 5129–5143.
35. Dunning, T.H. Gaussian Basis Sets for Use in Correlated Molecular Calculations. I. The Atoms Boron Through Neon and Hydrogen. *J. Chem. Phys.* **1989**, *90*, 1007–1023. https://doi.org/10.1063/1.456153.
36. Cordero, B.; Gomez, V.; Platero-Prats, A.E.; et al. Covalent Radii Revisited. *Dalton Trans.* **2008**, pp. 2832–2838.
37. Frisch, M.J.; Trucks, G.W.; Schlegel, H.B.; et al. *Gaussian 16*, Revision C.01; Gaussian Inc.: Wallingford, CT, USA, 2016.
38. Werner, H.J.; Knowles, P.J.; Manby, F.R.; et al. The Molpro Quantum Chemistry Package. *J. Chem. Phys.* **2020**, *152*, 144107.
39. Mata, S.; Peña, I.; Cabezas, C.; et al. A Broadband Fourier-Transform Microwave Spectrometer with Laser Ablation Source: The Rotational Spectrum of Nicotinic Acid. *J. Mol. Spectrosc.* **2012**, *280*, 91–96.
40. National Institute of Standards and Technology. NIST Chemistry WebBook, NIST Standard Reference Database Number 69. Available online: https://webbook.nist.gov/chemistry/ (accessed on 1 June 2026).
41. Alonso, J.L. Microwave Spectrum of Cyclohexanone. *J. Mol. Struct.* **1981**, *73*, 63–69.
42. Wachsmuth, D.; Jahn, M.K.; Blanco, S.; et al. Inversion of Bicyclic Decanes: Rotational Spectra of the Trans and Double Cis Conformations of 2-Decalone. *ChemPhysChem* **2017**, *18*, 3620–3624. https://doi.org/10.1002/cphc.201700848.
43. Craig, N.C.; Chen, Y.; Fuson, H.A.; et al. Microwave Spectra of the Deuterium Isotopologues of cis-Hexatriene and a Semiexperimental Equilibrium Structure. *J. Phys. Chem. A* **2013**, *117*, 9391–9400. https://doi.org/10.1021/jp311035c.
44. Lippincott, E.R.; Kenney, T.E. The Vibrational Spectra and Geometric Configuration of cis-1,3,5-Hexatriene. *J. Am. Chem. Soc.* **1962**, *84*, 3641–3648.
45. Rakovic, D.; Stepanyan, S.A.; Gribov, L.A.; et al. The Solution of the Inverse Spectroscopic Problem for the IR Spectra of trans- and cis-Hexatrienes. *J. Mol. Struct.* **1982**, *90*, 363–377.
46. Wang, X.; Zheng, Y.; Xu, X.; et al. Rotational Spectrum of Isochroman. *J. Mol. Struct.* **2022**, *1254*, 132322. https://doi.org/10.1016/j.molstruc.2021.132322.
47. Saxena, S.; Panchagnula, S.; Sanz, M.E.; et al. Structural Changes Induced by Quinones: High-Resolution Microwave Study of 1,4-Naphthoquinone. *ChemPhysChem* **2020**, *21*, 2579–2584. https://doi.org/10.1002/cphc.202000665.